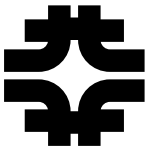

Fermi National Accelerator Laboratory

**FERMILAB-Pub-99/027-E**
**E835**

# Measurements of the Magnetic Form Factor of the Proton in the Timelike Region at Large Momentum Transfer

M. Ambrogiani et al.
The E835 Collaboration

*Fermi National Accelerator Laboratory*
*P.O. Box 500, Batavia, Illinois 60510*

February 1999

Submitted to *Physical Review D*

Operated by Universities Research Association Inc. under Contract No. DE-AC02-76CH03000 with the United States Department of Energy

## Disclaimer

*This report was prepared as an account of work sponsored by an agency of the United States Government. Neither the United States Government nor any agency thereof, nor any of their employees, makes any warranty, expressed or implied, or assumes any legal liability or responsibility for the accuracy, completeness, or usefulness of any information, apparatus, product, or process disclosed, or represents that its use would not infringe privately owned rights. Reference herein to any specific commercial product, process, or service by trade name, trademark, manufacturer, or otherwise, does not necessarily constitute or imply its endorsement, recommendation, or favoring by the United States Government or any agency thereof. The views and opinions of authors expressed herein do not necessarily state or reflect those of the United States Government or any agency thereof.*

## Distribution

*Approved for public release; further dissemination unlimited.*

## Copyright Notification

*This manuscript has been authored by Universities Research Association, Inc. under contract No. DE-AC02-76CHO3000 with the U.S. Department of Energy. The United States Government and the publisher, by accepting the article for publication, acknowledges that the United States Government retains a nonexclusive, paid-up, irrevocable, worldwide license to publish or reproduce the published form of this manuscript, or allow others to do so, for United States Government Purposes.*

# Measurements of the magnetic form factor of the proton in the timelike region at large momentum transfer

M. Ambrogiani[2], S. Bagnasco[6], W. Baldini[2], D. Bettoni[2], G. Borreani[6], A. Buzzo[3], R. Calabrese[2], R. Cester[6], P. Dalpiaz[2], X. Fan[5], G. Garzoglio[1], K. E. Gollwitzer[4], A. Hahn[1], S. Jin[5], J. Kasper[5], G. Lasio[4], M. Lo Vetere[3], E. Luppi[2], P. Maas[5], M. Macrì[3], M. Mandelkern[4], F. Marchetto[6], M. Marinelli[3], W. Marsh[1], M. Martini[2], E. Menichetti[6], R. Mussa[2], M.M. Obertino[6], M. Pallavicini[3], N. Pastrone[6], C. Patrignani[3], T.K. Pedlar[5], J. Peoples Jr.[1], S. Pordes[1], E. Robutti[3], J. Rosen[5], P. Rumerio[6], A. Santroni[3], M. Savrié[2], J. Schultz[4], K. K. Seth[5], G. Stancari[2], M. Stancari[4], J. Streets[1], A. Tomaradze[5], S. Werkema[1], and G. Zioulas[4]

[1] *Fermi National Accelerator Laboratory, Batavia, Illinois 60510*

[2] *Istituto Nazionale di Fisica Nucleare and University of Ferrara, 44100 Ferrara, Italy*

[3] *Istituto Nazionale di Fisica Nucleare and University of Genova, 16146 Genova, Italy*

[4] *University of California at Irvine, California 92717*

[5] *Northwestern University, Evanston, Illinois 60208*

[6] *Istituto Nazionale di Fisica Nucleare and University of Torino, 10125 Torino, Italy*

(Received 18 February 1999)

## Abstract

The cross section for the reaction $\bar{p}p \to e^+e^-$ has been measured at $s$ = 8.8, 10.8, 12.4, 13.1, and 14.4 GeV$^2$ by Fermilab experiment E835. A non-magnetic spectrometer is used to identify the $e^+e^-$ final states generated by the antiproton beam intersecting an internal hydrogen gas jet target. From the analysis of the 144 observed events, new high-precision measurements of the

proton magnetic form factor for timelike momentum transfers are obtained.

PACS numbers: 13.40.Gp, 13.75.Cs, 14.20.Dh

Typeset using REVTEX

## I. INTRODUCTION

The electromagnetic structure of the nucleon is directly probed by the measurement of electric and magnetic form factors, $G_E(q^2)$ and $G_M(q^2)$ as function of the squared four-momentum transfer $q^2$. The electric and magnetic form factors of the proton in the spacelike region ($q^2 < 0$) have been measured in elastic electron-proton scattering up to $|q^2| = 10$ (GeV/c)$^2$ and $|q^2| = 31$ (GeV/c)$^2$, respectively. Recent data can be found in Refs. [1–3]. Measurements of the form factors for timelike momentum transfers ($s = q^2 > 0$) are mainly concentrated in a small interval near threshold $4m_p^2c^4 \leq s \leq 7$ GeV$^2$ [4–12]. The first attempts to make measurements at larger momentum transfers were made by the CERN experiment R704, but they were only able to establish upper limits at $s = 8.9$ GeV$^2$ and 12.5 GeV$^2$ [13]. The first successful measurements were reported by the Fermilab experiment E760, which obtained $G_M$ at $s = 8.9$, 12.4 and 13.0 GeV$^2$ [14].

In this paper we present results from new, improved measurements of the cross section for the reaction:

$$\overline{p}p \to e^+e^- \tag{1}$$

in the center-of-mass (CM) energy interval 2.9 GeV $\leq \sqrt{s} \leq$ 4.3 GeV. The differential cross section for process (1) can be expressed in terms of the proton magnetic and electric form factors $G_M$ and $G_E$ as follows [15]:

$$\frac{d\sigma}{d(\cos\theta^*)} = \frac{\pi\alpha^2(\hbar c)^2}{8\,E\,P}\times \\ \times\left[|G_M|^2(1+\cos^2\theta^*) + \frac{4m_p^2c^4}{s}|G_E|^2\sin^2\theta^*\right], \tag{2}$$

where, in the CM frame, $E$ and $P$ are the energy and momentum of the antiproton, and $\theta^*$ is the angle between the electron and the antiproton.

## II. EXPERIMENTAL APPARATUS

Experiment E835 is dedicated to the study of charmonium by resonant formation in $\bar{p}p$ annihilations. It has been carried out at the antiproton accumulator of the Fermilab Antiproton Source and has taken data from October 1996 through September 1997. The charmonium physics program determined our choices of beam momentum and of integrated luminosity accumulated in each energy region.

The circulating beam of stochastically cooled antiprotons (up to $5 \times 10^{11}$ $\overline{p}$) intersects an internal hydrogen gas jet target [16] to provide average instantaneous luminosities of $2 \times 10^{31}$ cm$^{-2}$ s$^{-1}$. The interaction region, as determined by the intersection of the antiproton beam with the hydrogen gas jet, is approximately $(5 \times 5 \times 7)$ mm$^3$.

The E835 apparatus has been designed to detect electromagnetic final states. It makes use of some of the components employed in experiment E760 [14] as well as several upgrades. The layout of the detector is shown in Fig. 1. It is a non-magnetic spectrometer with full azimuthal ($\phi$) coverage and polar angle ($\theta$) acceptance ranging from 2° to 70° in the lab frame. The central detector ($11° < \theta < 70°$) has cylindrical symmetry around the beam axis; its main components are the lead glass calorimeter (CCAL), the threshold Čerenkov counter for $e/\pi$ discrimination, the inner tracking system and a luminosity monitor.

The central calorimeter [17] is a matrix of 1280 lead glass counters (64 in $\phi$ by 20 in $\theta$) pointing to the interaction region, measuring the energy and direction of electrons and photons. The CCAL has an energy resolution $\sigma_E/E = 0.014 + 0.06/\sqrt{E(\mathrm{GeV})}$ and an angular resolution (r.m.s.) of 11 mrad in $\phi$ and 6 mrad in $\theta$; these angular errors include the contribution due to the finite size of the interaction region. Each counter in CCAL is equipped with an ADC to measure pulse height and a TDC to provide timing information to reject pile-up. All showers with energy above 80 MeV can be identified as 'in time' or 'out of time'. Showers with lower energy sometimes have no TDC information and are then labeled 'undetermined'.

The Čerenkov counter [18] contains 16 cells (8 in $\phi$ by 2 in $\theta$) and covers the full azi-

muth and from 15° to 65° in $\theta$. Each channel is connected to an ADC. The counter is a threshold device and serves to identify electrons and to reject pions at the trigger level, and to distinguish single electrons from electron-positron pairs in the analysis.

The inner tracking system consists of two layers of straw tube drift chambers (SC1 and SC2) [19] for the measurement of $\phi$ and a scintillating fiber tracker (SF) with VLPC readout [20] for the measurement of $\theta$. The angular resolution of the inner tracking system is 11 mrad in $\phi$, whereas in $\theta$ it varies from 3 mrad at small angles to 11 mrad at large angles. The intrinsic resolution of the scintillating fiber detector is better than 2 mrad, but the $\theta$ resolution is dominated by the size of the interaction region.

Three cylindrical plastic scintillator hodoscopes (H1, H2$'$ and H2) located at increasing distances from the beam axis are used for triggering. The pulse heights, together with those in the Čerenkov counter, are used to distinguish singly charged particles from electron-positron pairs due to $\gamma$ conversions and to $\pi^0$ Dalitz decays.

The polar angle region from 2° to 12° is covered by a planar forward calorimeter and a plastic scintillator hodoscope, not used in this analysis.

The measurement of the luminosity is provided by three silicon detectors positioned at $\theta = 86.5°$ to the $\overline{p}$ beam direction, measuring the yield of elastic recoil protons. The errors in the absolute luminosity measurements are estimated to be less than $\pm 2.5\%$.

The experiment uses the DART data acquisition system to acquire and store data [21]. At a typical luminosity the first level trigger rate is 1 kHz and the live-time is greater than 90%.

## III. TRIGGER AND EVENT SELECTION

In this experiment, $e^+e^-$ cross sections of a few picobarns must be measured in presence of a $\approx 60$ mb total cross section, i.e. a rejection factor of the order of $10^{10}$ must be achieved.

The first level trigger for $e^+e^-$ events requires two electrons, each defined by a coincidence between the appropriate azimuthal elements of H1, H2 and the corresponding cells of

the Čerenkov counter; independently, two high-energy showers are required in the central calorimeter, with an azimuthal opening angle greater than 90°.

Events which satisfy the hardware trigger are processed by the on-line filter, which selects events in which the two highest-energy clusters in the CCAL have an invariant mass greater than 2 GeV/c$^2$.

Electron tracks are reconstructed off-line by associating hodoscope hits, Čerenkov counter signals and calorimeter showers. Track information from the inner detectors is added to improve the angular resolution. The two electron candidates are identified as the tracks with the highest invariant mass. The selection of $\overline{p}p \to e^+e^-$ proceeds in four steps.

*a. Electron identification.* For each candidate electron track, an electron weight index (ELW) is constructed using the pulse heights in the H1, H2, H2′ and Čerenkov counters, second moments of the transverse shower distribution in CCAL and the fractional shower energy in a $3 \times 3$ block region of CCAL. ELW is a likelihood ratio for the electron hypothesis versus the background hypothesis. Since in a good event both candidates are required to be good electron tracks, a sensible variable to use is the product of the ELW indices of the two candidate electrons. The distribution of $\log_{10}(\mathrm{EW1} \cdot \mathrm{EW2})$ in a clean electron sample is shown in Fig. 2. In order to reduce the size of the data sample, a preliminary selection is applied to the raw data by imposing a loose cut on the product of the ELW for the two electron candidates ($ELW1 \times ELW2 > 0.1$): only events which pass this preliminary selection undergo the subsequent analysis. In the final selection, the electron weight cut is $ELW1 \times ELW2 > 1$.

*b. Fiducial volume.* The cut in fiducial volume is necessary in order to remove inhomogeneities in the response of the detector at its edges. For this reason we accept only events in which the two electron candidates have polar angles in the interval $15^\circ < \theta < 60^\circ$, well within the angular coverage of CCAL and of the Čerenkov counter.

*c. CCAL multiplicity.* To avoid rejecting events in which the electron or positron radiates a Bremsstrahlung photon which forms a distinct cluster in the CCAL, we do not impose

a strict cut demanding only two in-time clusters. Events with more than two in-time clusters are kept provided that the extra clusters, when paired with either electron candidate, give an invariant mass below 100 MeV/c$^2$. In addition, any number of out-of-time or undetermined clusters is allowed.

*d. Kinematical fit.* The goodness of the two body hypothesis is finally tested by means of a four constraint kinematical fit. All candidate events are tested with this hypothesis and are accepted if the fit probability is above 1%.

The number $N$ of events selected with these criteria is shown in Table I for each energy region.

## IV. EFFICIENCIES

The overall efficiency $\varepsilon$ is the product of the trigger efficiency ($\varepsilon_{\rm tri}$) and the efficiencies of the preliminary selection ($\varepsilon_{\rm pre}$) and of the off-line analysis ($\varepsilon_{\rm ana}$): $\varepsilon = \varepsilon_{\rm tri} \cdot \varepsilon_{\rm pre} \cdot \varepsilon_{\rm ana}$.

The trigger efficiency $\varepsilon_{\rm tri}$ has been measured with a special trigger run at the $J/\psi$ energy, which required only one electron track in the H1, H2 and Čerenkov counters, in addition to the two cluster requirement in the central calorimeter; the result is $\varepsilon_{\rm tri} = 0.898 \pm 0.005$.

The efficiency of the preliminary off-line cut $ELW1 \times ELW2 > 0.1$ has been measured using clean samples of $J/\psi \to e^+e^-$ and $\psi' \to e^+e^-$ events selected by means of topological cuts and a kinematical fit and has been found to be $\varepsilon_{\rm pre} = 0.966 \pm 0.001$.

The efficiency of the second set of off-line cuts has been evaluated at the $J/\psi$ and $\psi'$ energies. Figure 3 shows the invariant mass distribution for candidate electrons after preliminary cuts only (a) at the $J/\psi$ and (b) at the $\psi'$ formation energies. The cross-hatched areas in both histograms show the background contamination in these samples, calculated by applying the same analysis to data taken off resonance and rescaled by luminosity. In Fig. 3(b) inclusive $J/\psi X$ events coming from the decay $\psi' \to J/\psi + X$ are also shown (horizontal lines). They are selected by means of a 1C kinematical fit on events with an identified $e^+e^-$ pair in the final state ($ELW1 \times ELW2 > 1$), requiring that the fit probability be higher than

1%, with the additional requirement that the fit probability for the hypothesis $\psi' \to e^+e^-$ be less than 10%. These inclusive events have been rescaled by the efficiency of this inclusive selection ($\simeq 95\%$) and subtracted. Figure 4 shows the corresponding distributions after complete event selection. It can be seen that the background contamination in these data samples is very low.

The efficiency of the off-line analysis is defined as the fraction of events in the preliminary samples (Fig. 3) that survive all cuts (Fig. 4), once background (including $J/\psi\, X$ events at the $\psi'$) is subtracted. At the $\psi'$, only events with invariant mass above 3.4 GeV are considered. The efficiency calculated in this way is found to be $0.777 \pm 0.004$ at the $J/\psi$ and $0.75 \pm 0.01$ at the $\psi'$. A single value of $\varepsilon_{\rm ana} = 0.764 \pm 0.003(\rm stat) \pm 0.045(\rm syst)$ is used for the measurement of the form factor, where the systematic error takes into account the difference in efficiency found at the $J/\psi$ and at the $\psi'$, the variation of efficiency with time and the effect of the background subtraction procedure. The overall efficiency used at all energies is thus $\varepsilon = 0.663 \pm 0.005(\rm stat) \pm 0.05(\rm syst)$.

## V. BACKGROUND STUDIES

The main sources of background for the reaction $\overline{p}p \to e^+e^-$ are photon conversions and $\pi^0$ Dalitz decays, two body hadronic final states (mainly $\pi^+\pi^-$) and inclusive $J/\psi\, X$ events.

*a. Photon conversions and Dalitz decays.* We consider the reactions:

$$\bar{p}p \to \pi^0\pi^0 \tag{3}$$

$$\bar{p}p \to \pi^0\gamma \tag{4}$$

$$\bar{p}p \to \gamma\gamma. \tag{5}$$

Two coalescing electron-positron pairs are generated if the two photons in reaction 5 convert in matter. A back-to-back electron-positron pair can be produced from reaction 4 as well and in two ways: a) the pion decays into two photons, one of which converts in matter; b) the pion undergoes Dalitz decay ($\pi^0 \to e^+e^-\gamma$). In both cases, the original photon has to

convert and one of the photons from the pion has to be undetected. A similar reasoning applies to reaction 3. The backgrounds due to reactions 3 and 4 via the mechanism just described (feed-down) are much bigger than the one arising from process 5. The probability of a photon to convert before hodoscope H1, and thus be able to fire the first-level trigger, has been measured in a sample of $\pi^0\pi^0$ events collected with a special total-energy trigger with no hodoscope veto; it is $\eta < 1.7 \times 10^{-2}$, and it is consistent with estimates that employ the thickness of the material between the interaction region and H1. $\delta = 1.2 \times 10^{-2}$ is the probability of a pion to decay through the Dalitz process. The feed-down backgrounds from $\pi^0\pi^0$ and $\pi^0\gamma$ to $\gamma\gamma$ ($\sigma'_{\pi^0\pi^0}$ and $\sigma'_{\pi^0\gamma}$, respectively) have been estimated in E760 with Monte Carlo techniques [22], and they dominate over the $\bar{p}p \to \gamma\gamma$ continuum cross section. The low probability of not detecting two photons from $\pi^0\pi^0$ is compensated by the high $\bar{p}p \to \pi^0\pi^0$ cross section, making these two feed-down sources of comparable magnitude.

Since the energy deposit spectra of single and double tracks overlap, the electron-positron pairs might be misidentified as single electron tracks. The rejection power of the ELW cut has been estimated on a sample of 'pairs', defined as charged tracks with a large energy deposit in the CCAL that, combined with another calorimeter cluster, give a $\pi^0$ invariant mass. The probability $\omega$ that an event with two back-to-back pairs satisfies the ELW cut is $\omega < 4 \times 10^{-2}$ (Fig. 5).

From the above discussion, the expected background cross section due to processes 3, 4 and 5 is:

$$\begin{aligned} \sigma_p < \omega \cdot \Big[ & (\delta + 2\eta)^2 \ \sigma'_{\pi^0\pi^0} \ + \\ & (\delta + 2\eta)\eta \ \sigma'_{\pi^0\gamma} \ + \\ & \eta^2 \qquad \sigma_{\gamma\gamma} \qquad \Big]. \end{aligned} \tag{6}$$

Numerically, $\sigma_p$ is less than $6 \times 10^{-2}$ pb at 2.9 GeV and less than $3 \times 10^{-3}$ pb at 3.5 GeV.

*b. Hadronic two-body.* A two-body hadronic final state can simulate an $e^+e^-$ final state if the Čerenkov gives a signal and a hadronic shower is generated in the CCAL with the characteristics of an EM shower (energy and shape). Because of its high cross section and the high velocity of the pions, the process:

$$\bar{p}p \to \pi^+\pi^- \tag{7}$$

is the most relevant. The probability $\xi$ of a hadronic shower being generated in the CCAL with an energy compatible with the $e^+e^-$ hypothesis has been measured with data from a dedicated trigger, requiring two charged tracks as defined by the hodoscopes, without any requirements on the Čerenkov or the CCAL; the result is $\xi = 1 \times 10^{-2}$. From the same sample of data, the rejection inefficiency of the Čerenkov contribution to the ELW cut comes out to be $\kappa < 5 \times 10^{-3}$ per track. The differential cross section of process 7 integrated over the acceptance $\alpha_{acc}$ of the E835 detector varies between 2 $\mu$b (at 2.9 GeV) and 0.5 $\mu$b (at 3.6 GeV). The expected background is

$$\begin{aligned} \sigma_h &< (\alpha_{acc}\sigma_{\pi^+\pi^-}) \cdot \kappa^2 \cdot \xi^2 \\ &= 0.5 \times 10^{-2} \text{ pb (at 2.9 GeV)} \\ &= 1.3 \times 10^{-3} \text{ pb (at 3.6 GeV).} \end{aligned} \tag{8}$$

*c. Inclusive $J/\psi\, X$.* Above a certain threshold, the process $\bar{p}p \to J/\psi + X$ followed by $J/\psi \to e^+e^-$ can fit the $e^+e^-$ two-body kinematics, when $X$ is not detected. For this reason, data taken in proximity of some charmonium resonances has been excluded from the data sample for this analysis. The remaining $J/\psi$-inclusive continuum observable by this experiment is less than 5 pb and is mainly due to $\bar{p}p \to J/\psi\ \pi^0 \to e^+e^-\gamma\gamma$ [23]. The probability for an inclusive event to satisfy two-body kinematics has been evaluated at the $\chi_{c1}$ and $\chi_{c2}$ resonances. The result is $5 \times 10^{-3}$ and will be taken as an upper limit for all inclusive processes in the whole energy range. This yields a background contribution $\sigma_i$ less than $2.5 \times 10^{-2}$ pb.

Summing all the contributions $\sigma_B = \sigma_p + \sigma_h + \sigma_i$, one obtains upper limits on the expected background cross section of $9.0 \times 10^{-2}$ pb at 2.9 GeV and $2.9 \times 10^{-2}$ pb at 3.5 GeV, corresponding to approximately one event at both energies.

Since our background estimates are conservative, no subtraction from the number of candidate events is performed.

## VI. MEASUREMENT OF THE MAGNETIC FORM FACTOR OF THE PROTON

The number $N$ of events collected with an integrated luminosity $L$ and an overall efficiency $\varepsilon$ is

$$N = \varepsilon \; L \; \sigma_{acc}, \tag{9}$$

where the term $\sigma_{acc}$ is the differential cross section integrated over the CM acceptance region:

$$\sigma_{acc} \equiv \int_{-|\cos\theta^*|_{\max}}^{+|\cos\theta^*|_{\max}} \left[\frac{d\sigma}{d(\cos\theta^*)}\right] d(\cos\theta^*) \tag{10}$$

$$= \frac{\pi\alpha^2(\hbar c)^2}{8EP} \cdot \left[A \cdot |G_M|^2 + \frac{4m_p^2c^4}{s} \cdot B \cdot |G_E|^2\right]. \tag{11}$$

At different values of $s$, the fiducial range $15^\circ < \theta < 60^\circ$ used in the event selection corresponds to different acceptances for $\theta^*$. At $\sqrt{s} < 3.661$ GeV, it is the upstream edge of the fiducial range ($\theta = 60^\circ$) that determines $|\cos\theta^*|_{\max}$; whereas for $\sqrt{s} > 3.661$ GeV it is the downstream edge ($\theta = 15^\circ$) that constrains the acceptance. The fact that the E835 apparatus cannot distinguish between electrons and positrons is taken into account by integrating from $-|\cos\theta^*|_{\max}$ to $+|\cos\theta^*|_{\max}$; the acceptance coefficients $A$ and $B$ are:

$$A \equiv 2 \cdot \int_0^{|\cos\theta^*|_{\max}} \left(1 + \cos^2\theta^*\right) d(\cos\theta^*) \tag{12}$$

$$B \equiv 2 \cdot \int_0^{|\cos\theta^*|_{\max}} \left(1 - \cos^2\theta^*\right) d(\cos\theta^*). \tag{13}$$

For small $|\cos\theta^*|_{\max}$, $A$ is approximately equal to $B$ and the relative importance of the 'electric' and 'magnetic' contributions is weighted by $4m_p^2c^4/s$ only. As $|\cos\theta^*|_{\max}$ approaches one, the ratio $A/B$ tends to 2, and the 'electric' contribution is further suppressed. Since the small number of events and the limited $\cos\theta^*$ range do not allow us to measure the angular distribution, two alternative hypotheses have been made: (a) $|G_E| = |G_M|$, as is the case at the threshold of the timelike region ($s = 4m_p^2c^4$); (b) the 'electric' contribution is assumed to be negligible. Under hypothesis (b), the measurement of the magnetic form factor of the proton is achieved through the relation:

$$|G_M| = \frac{1}{\alpha\,(\hbar c)} \cdot \sqrt{\frac{8}{\pi}} \cdot \left[\frac{E\ P\ N}{\varepsilon\ A\ L}\right]^{\frac{1}{2}}. \tag{14}$$

Under hypothesis (a), $A$ is replaced by $A + (4m_p^2c^4/s) \cdot B$. The results obtained are shown in Table I. It should be observed that the values of $|G_M|$ determined in the two hypotheses differ by less than 15%. The values of $|G_M|$ obtained under assumption (a) are plotted in Fig. 6, where they are compared with E760 results and with earlier measurements [4–8,10–14]. It can be seen that the E835 data are in excellent agreement with the E760 results and that they have a much better accuracy. Some data have been taken above the $\psi'$ resonance at $s = 18.4$ GeV$^2$. No $e^+e^-$ events have been observed. In Table I an upper limit on the form factor is given corresponding to a 90% confidence level [24]. Figure 6 shows a fit to the data in the form

$$|G_M| = \frac{C}{s^2\ \ln^2(s/\Lambda^2)} \tag{15}$$

where $\Lambda = 0.3$ GeV is the QCD scale parameter and $C$ is a free parameter (dashed line). This functional form comes from the perturbative QCD prediction that for large momentum transfers $q^4|G_M|$ should be nearly proportional to the square of the running coupling constant for strong interactions $\alpha_s^2(q^2)$ [25,26]. It can be seen that the fit reproduces the main $q^2$ dependence of the data over the entire range explored so far. The dipole behavior of the form factors in the spacelike region for the same values of $\left|q^2\right|$ is also plotted in Fig. 6 (dot-dashed line). It is to be noted that the numerical values of $|G_M|$ in the region explored by this experiment are approximately twice as large as those in the corresponding spacelike region, consistent with the findings of E760 [14] and with calculations based on the quark-diquark model of the proton [27].

## VII. CONCLUSIONS

We have presented new, high-precision measurements of the proton magnetic form factor in the timelike region at high $q^2$. The results obtained are in excellent agreement with previous measurements and follow the semi-quantitative predictions of QCD.

## VIII. ACKNOWLEDGEMENTS

We gratefully acknowledge the technical support from our collaborating institutions and the contribution of the Fermilab Beams Division. This work was supported in part by the U.S. Department of Energy, the U.S. National Science Foundation and the Italian Istituto Nazionale di Fisica Nucleare.

# REFERENCES


[1] A. F. Sill *et al.*, Phys. Rev. D **48**, 29 (1993).

[2] R. C. Walker *et al.*, Phys. Rev. D **49**, 5671 (1994).

[3] L. Andivahis *et al.*, Phys. Rev. D **50**, 5491 (1994).

[4] M. Conversi *et al.*, Il Nuovo Cimento **XL A**, 690 (1965).

[5] D. L. Hartill *et al.*, Phys. Rev. **184**, 1415 (1969).

[6] M. Castellano *et al.*, Il Nuovo Cimento **14 A**, 1 (1973).

[7] G. Bassompierre *et al.*, Phys. Lett. **68B**, 477 (1977).

[8] B. Delcourt *et al.*, Phys. Lett. **86B**, 395 (1979).

[9] D. Bisello *et al.*, Nucl. Phys. **B224**, 379 (1983).

[10] D. Bisello *et al.*, Z. Phys. **48**, 23 (1990).

[11] G. Bardin *et al.*, Nucl. Phys. **B411**, 3 (1994).

[12] A. Antonelli *et al.*, Phys. Lett. B **334**, 431 (1994).

[13] C. Baglin *et al.*, Phys. Lett. **163B**, 400 (1985).

[14] T. A. Armstrong *et al.*, Phys. Rev. Lett. **70**, 1212 (1993).

[15] A. Zichichi *et al.*, Il Nuovo Cimento **XXIV**, 170 (1962).

[16] D. Allspach *et al.*, Nucl. Instrum. Meth. **A 410**, 195 (1998).

[17] L. Bartoszek *et al.*, Nucl. Instrum. Meth. **A 301**, 47 (1991).

[18] C. Biino *et al.*, Nucl. Instrum. Meth. **A 317**, 135 (1992).

[19] S. Bagnasco *et al.*, Nucl. Instrum. Meth. **A 409**, 75 (1998).

[20] M. Ambrogiani *et al.*, IEEE Trans. Nucl. Sci. **44**, 460 (1997).

[21] G. Oleynik *et al.*, IEEE Trans. Nucl. Sci. **41**, 45 (1994).

[22] T. A. Armstrong *et al.*, Phys. Rev. D **56**, 2509 (1997).

[23] T. A. Armstrong *et al.*, Phys. Rev. Lett. **69**, 2337 (1992).

[24] G. J. Feldman and R. D. Cousins, Phys. Rev. D **57**, 3873 (1998).

[25] G. Lepage and S. Brodsky, Phys. Rev. Lett. **43**, 545 (1979).

[26] G. Lepage and S. Brodsky, Phys. Rev. D **22**, 2157 (1980).

[27] P. Kroll *et al.*, Phys. Lett. B **316**, 546 (1993).

## TABLES

| $s$ | $L$ | $N$ | $\sigma_{acc}$ | $\lvert\cos\theta^*\rvert_{\max}$ | $10^2 \times \lvert G_M \rvert$ | |
|---|---|---|---|---|---|---|
| $(\mathrm{GeV}^2)$ | $(\mathrm{pb}^{-1})$ | | (pb) | | (a) | (b) |
| $8.84 \pm 0.16$ | 17.69 | 93 | $7.93^{+0.82+1.00}_{-0.82-0.69}$ | 0.451 | $3.59^{+0.18+0.23}_{-0.19-0.17}$ | $4.17^{+0.21+0.26}_{-0.22-0.19}$ |
| $10.78 \pm 0.28$ | 1.78 | 3 | $2.5^{+1.9+0.3}_{-1.6-0.2}$ | 0.544 | $2.13^{+0.70+0.15}_{-0.84-0.11}$ | $2.40^{+0.79+0.15}_{-0.95-0.12}$ |
| $12.43 \pm 0.02$ | 47.84 | 33 | $1.04^{+0.18+0.13}_{-0.18-0.09}$ | 0.601 | $1.43^{+0.12+0.09}_{-0.13-0.07}$ | $1.58^{+0.13+0.10}_{-0.14-0.07}$ |
| $13.11 \pm 0.18$ | 33.99 | 14 | $0.62^{+0.19+0.08}_{-0.16-0.05}$ | 0.621 | $1.12^{+0.16+0.07}_{-0.16-0.06}$ | $1.24^{+0.18+0.08}_{-0.18-0.06}$ |
| $14.36 \pm 0.50$ | 1.86 | 1 | $0.8^{+1.4+0.1}_{-0.5-0.1}$ | 0.604 | $1.39^{+0.91+0.13}_{-0.54-0.11}$ | $1.51^{+1.00+0.14}_{-0.59-0.12}$ |
| $18.40 \pm 0.01$ | 0.76 | 0 | $< 4.88$ | 0.508 | $< 4.40$ | $< 4.74$ |

TABLE I. Summary of the results of the form factor analysis. For each energy region, the integrated luminosity $L$, the number of selected events $N$, the cross section $\sigma_{acc} \equiv N/(L\varepsilon)$ and the geometrical acceptance in the CM frame are shown. The results correspond to the two hypotheses described in the text: (a) $|G_E| = |G_M|$ and (b) negligible 'electric' contribution. An upper limit at the 90% confidence level is reported where there are no observed events. The errors shown are statistical and, respectively, systematic. The systematic uncertainty is due to the errors on efficiency and luminosity. The error on $s$, due to the grouping of several runs at different energies, is also included in the systematic error. The various contributions to the systematic errors are added linearly.

## FIGURES

FIG. 1. The E835 detector layout.

FIG. 2. Distributions of the product of ELW indices for electrons from a clean sample of $J/\psi \to e^+e^-$ decays.

FIG. 3. Invariant mass distribution for candidate electrons after preliminary cuts only: (a) at the $J/\psi$ formation energy (white) and at $\sqrt{s} = 3.3$ GeV (cross-hatched, rescaled by luminosity); (b) at the $\psi'$ formation energy (white, all events; horizontal lines, $J/\psi$-inclusive subsample) and at $\sqrt{s} = 3.8$ GeV (cross-hatched, rescaled by luminosity).

FIG. 4. Invariant mass distribution for candidate electrons after the whole selection: (a) at the $J/\psi$ formation energy (white) and at $\sqrt{s} = 3.3$ GeV (cross-hatched, rescaled by luminosity); (b) at the $\psi'$ formation energy (white, all events; horizontal lines, $J/\psi$-inclusive subsample) and at $\sqrt{s} = 3.8$ GeV (cross-hatched, rescaled by luminosity).

FIG. 5. (a) Distribution of the ELW index for events with two electron-positron pairs. (b) Rejection power $\omega$ as a function of the ELW cut for the same sample of events. The arrows indicate the actual cut used in the analysis.

FIG. 6. All existing measurements of the magnetic form factor of the proton, including the results of this experiment ($\bullet$). All values correspond to the $|G_E| = |G_M|$ hypothesis. A few upper limit values quoted in the text have been omitted for clarity. The dashed and dot-dashed curves are explained in the text.

Figure 1 Ambrogiani PRD

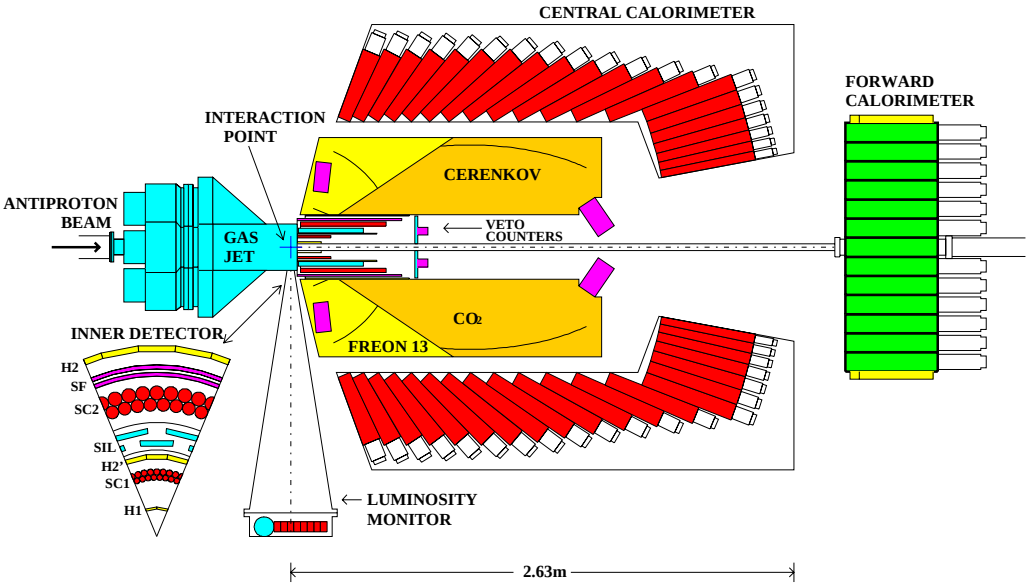

Figure 2 Ambrogiani PRD

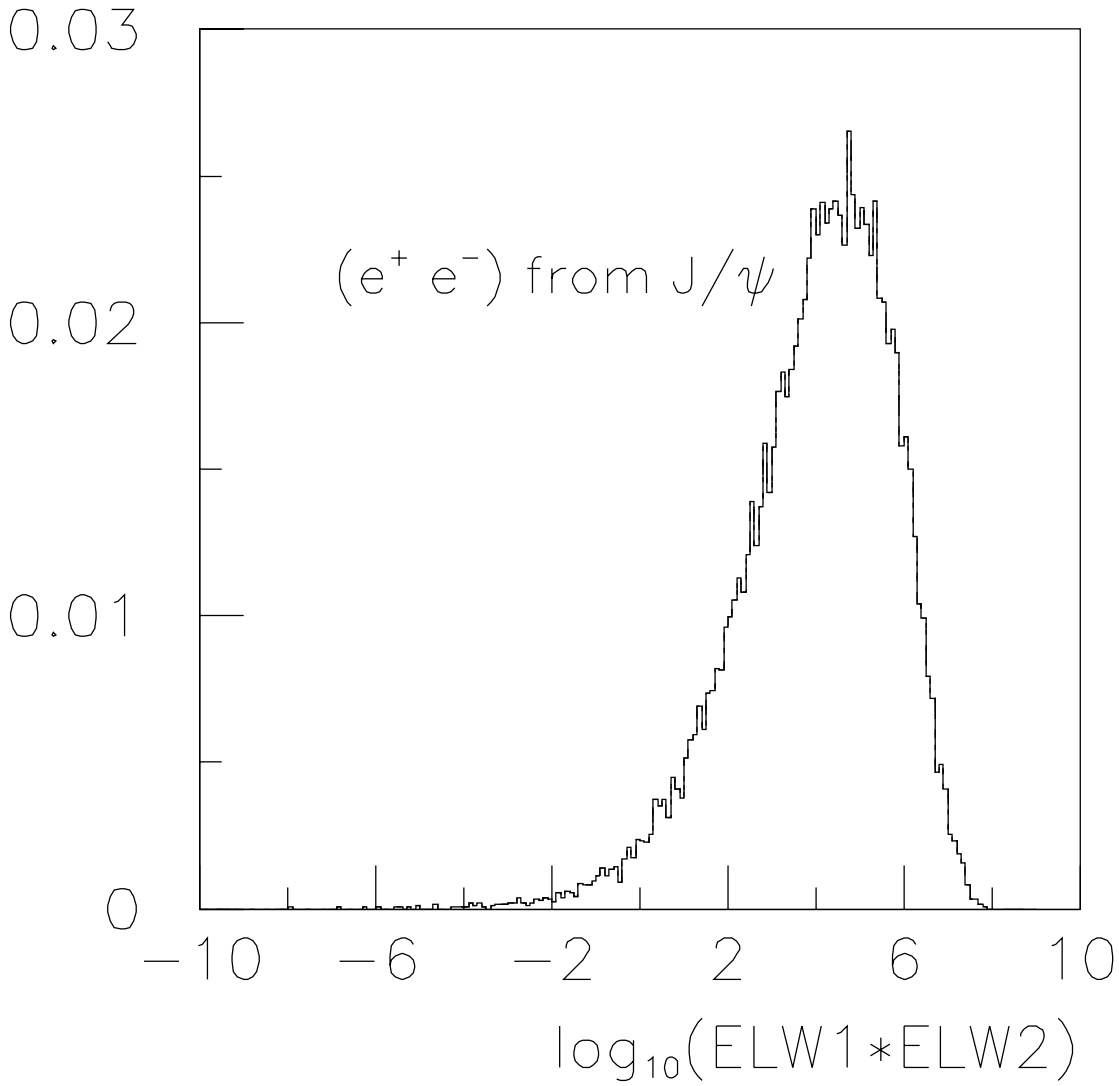

Figure 3(a) Ambrogiani PRD

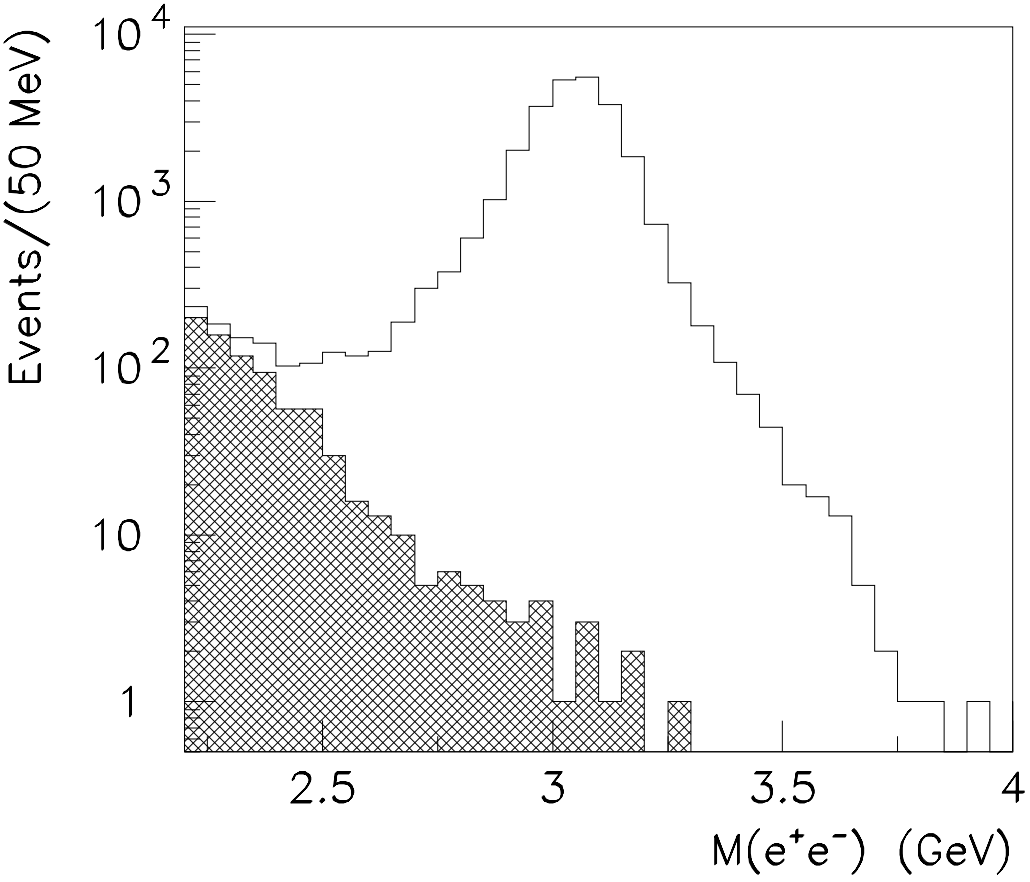


(a)

Figure 3(b) Ambrogiani PRD

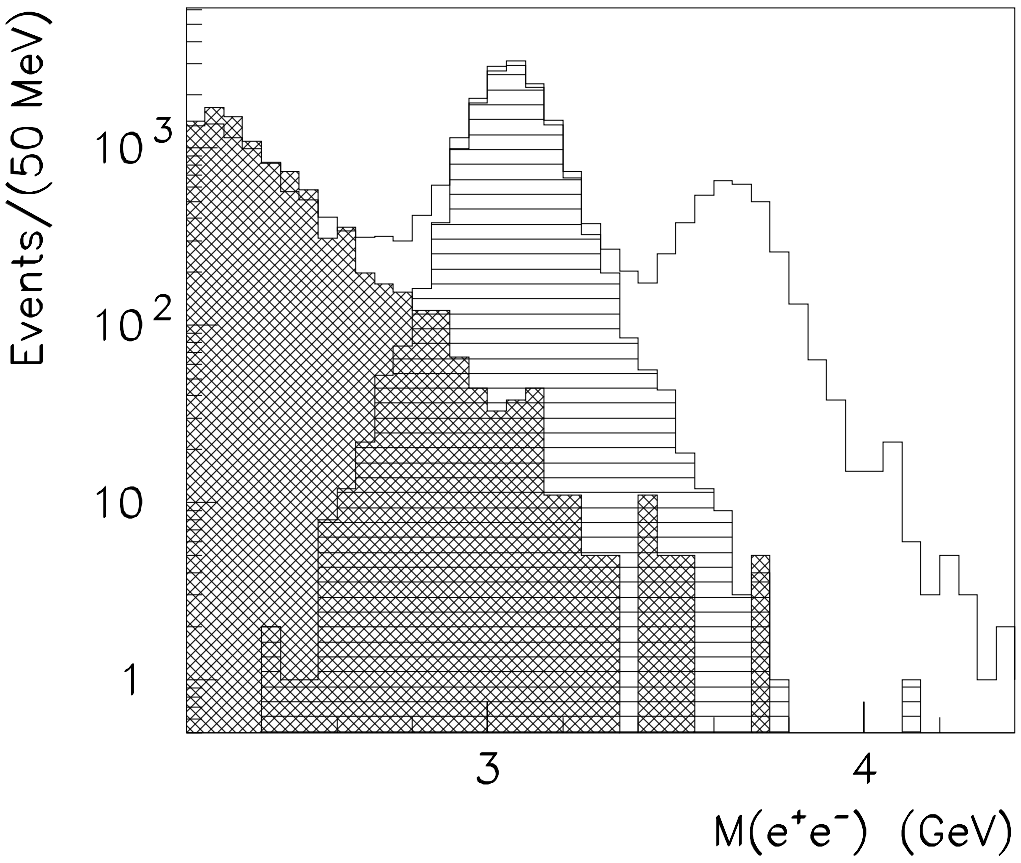


(b)

Figure 4(a) Ambrogiani PRD

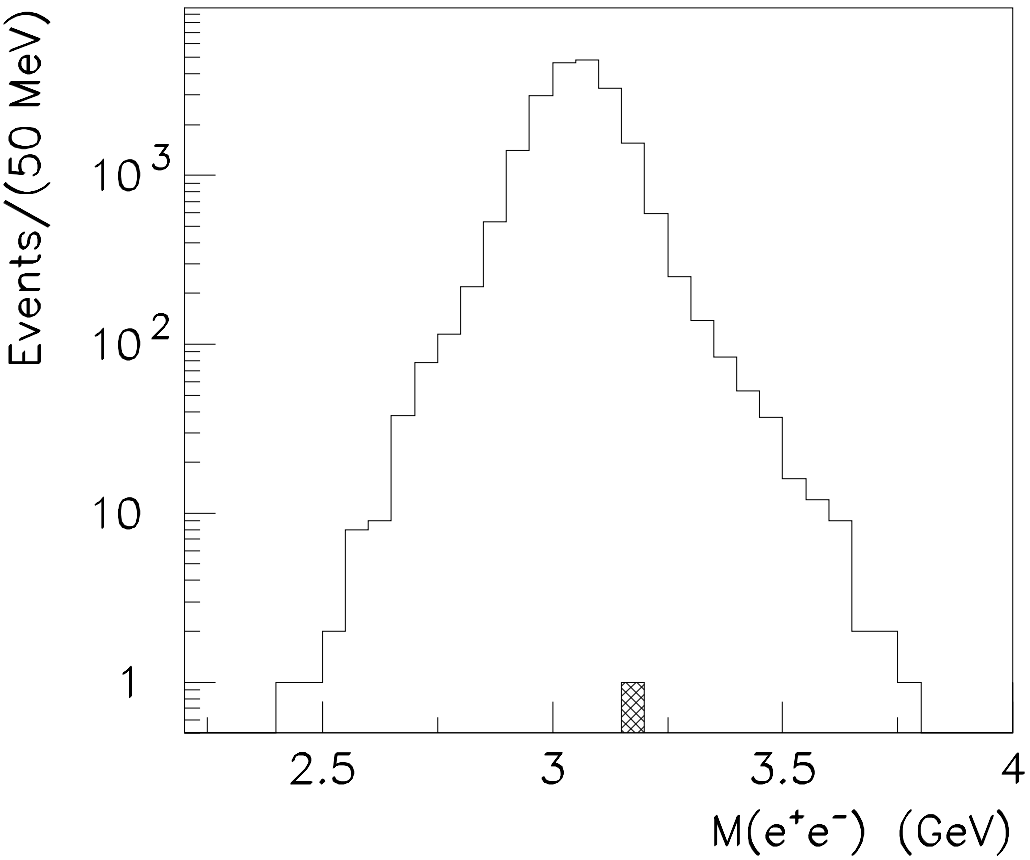


(a)

Figure 4(b) Ambrogiani PRD

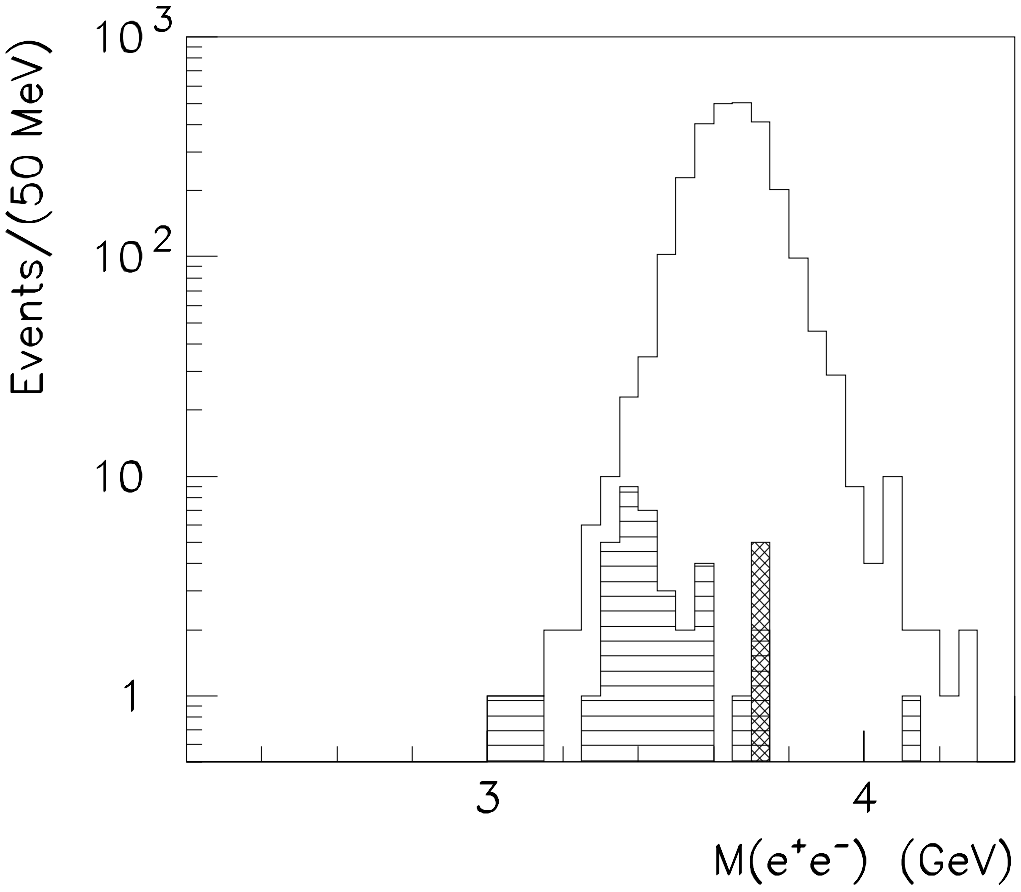


(b)

Figure 5 Ambrogiani PRD

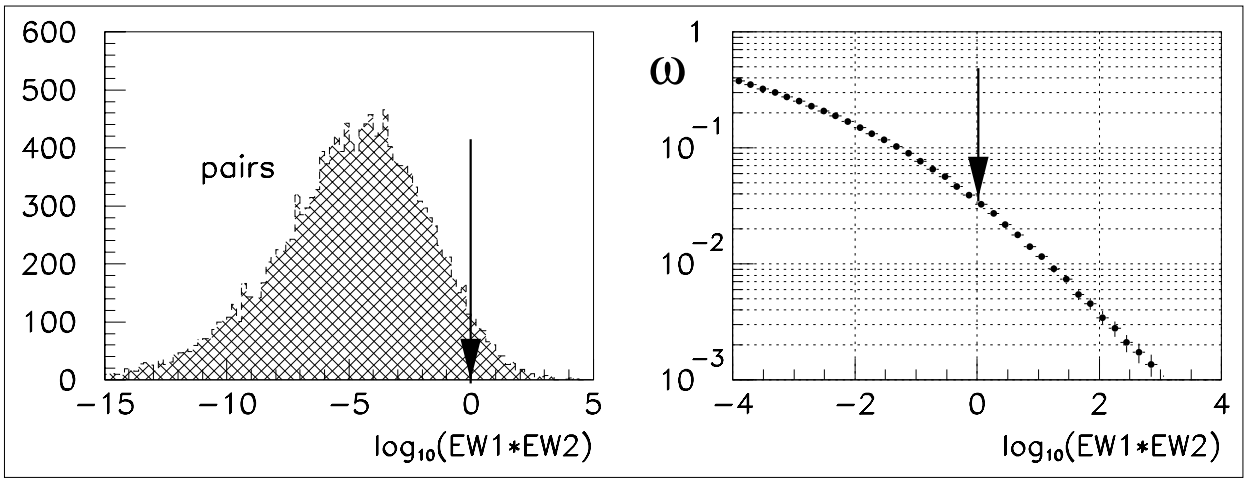


(a) (b)

Figure 6 Ambrogiani PRD